AD-A245 286

College of Earth and Mineral Sciences

PENNSTATE

ANNUAL REPORT

to

OFFICE OF NAVAL RESEARCH

Contract USN 00014-91-J-1189

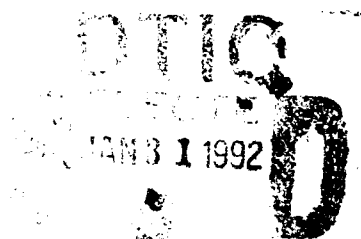January 1992

PREDICTION OF HYDROGEN ENTRY AND PERMEATION IN METALS AND ALLOYS

H. W. Pickering

Department of Materials Science and Engineering
The Pennsylvania State University

JAN 3 1 1992

92-02373

PENN STATE
College of Earth and Mineral Sciences

Undergraduate Majors

Ceramic Science and Engineering, Fuel Science, Metals Science and Engineering, Polymer Science; Mineral Economics; Mining Engineering, Petroleum and Natural Gas Engineering; Earth Sciences, Geosciences; Geography; Meteorology.

Graduate Programs and Fields of Research

Ceramic Science and Engineering, Fuel Science, Metals Science and Engineering, Polymer Science; Mineral Economics; Mining Engineering, Mineral Processing, Petroleum and Natural Gas Engineering; Geochemistry and Mineralogy, Geology, Geophysics; Geography; Meteorology.

Universitywide Interdisciplinary Graduate Programs Involving EMS Faculty and Students

Earth Sciences, Ecology, Environmental Pollution Control Engineering, Mineral Engineering Management, Solid State Science.

Associate Degree Programs

Metallurgical Engineering Technology (Shenango Valley Campus).

Interdisciplinary Research Groups Centered in the College

C. Drew Stahl Center for Advanced Oil Recovery, Center for Advanced Materials, Coal Research Section, Earth System Science Center, Mining and Mineral Resources Research Institute, Ore Deposits Research Group.

Analytical and Characterization Laboratories (Mineral Constitution Laboratories)

Services available include: classical chemical analysis of metals and silicate and carbonate rocks; X-ray diffraction and fluorescence; electron microscopy and diffraction; electron microprobe analysis; atomic absorption analysis; spectrochemical analysis; surface analysis by secondary ion mass spectrometry (SIMS); and scanning electron microscopy (SEM).

REPORT DOCUMENTATION PAGE

Public reporting burden for this collection of information is estimated to average 1 hour per response, including the time for reviewing instructions, searching existing data sources, gathering and maintaining the data needed, and completing and reviewing the collection of information. Send comments regarding this burden estimate or any other aspect of this collection of information, including suggestions for reducing this burden to Washington Headquarters Services, Directorate for Information Operations and Reports, 1215 Jefferson Davis Highway, Suite 1204, Arlington, VA 22202-4302, and to the Office of Management and Budget, Paperwork Reduction Project (0704-0188), Washington, DC 20503

1. AGENCY USE ONLY (Leave blank)	2. REPORT DATE January 1992	3. REPORT TYPE AND DATES COVERED Annual 10/1/90 to 9/30/91

4. TITLE AND SUBTITLE

Predictions of Hydrogen Entry and Permeation in Metals and Alloys

5. FUNDING NUMBERS

N00014-91-J-1189
431 5098

6. AUTHOR(S)

Howard W. Pickering

7. PERFORMING ORGANIZATION NAME(S) AND ADDRESS(ES)

The Pennsylvania State University
Department of Materials SCience & Engineering
326 Steidle Building
University Park, PA 16802

8. PERFORMING ORGANIZATION REPORT NUMBER

9. SPONSORING/MONITORING AGENCY NAME(S) AND ADDRESS(ES)

Scientific Officer
Materials Division Code: 1131M
Office of Naval Research
Arlington, VA 22217-5000
ATTN: A. John Sedriks

10. SPONSORING/MONITORING AGENCY REPORT NUMBER

11. SUPPLEMENTARY NOTES

12a. DISTRIBUTION/AVAILABILITY STATEMENT

Approved for public release; distribution is unlimited.

12b. DISTRIBUTION CODE

13. ABSTRACT (Maximum 200 words)

This report summarizes results of the past year on our continuing in-situ experiments directed to the problem of hydrogen entry and degradation of materials both for planar surfaces and for the more complicated recessed surface. For the planar surface the hydrogen permeation and scanning tunneling microscopy (STM) techniques are being used, and for the recessed surface the study uses a combined microscopy/electrochemical probe technique and a crevice geometry.

Further modeling of the hydrogen permeation technique has led to an experimental procedure that yields two previously unattainable rate constants that are important for controlling hydrogen absorption into a material from an aqueous environment, the hydrogen absorption (entry) and desorption (exiting) constants. STM has been further developed for in-situ study of hydrogen bonding at the atomic scale by successfully imaging hydrogen adsorption on the model $Si(100)2X1$ surface from a low pressure hydrogen gas phase. For the recessed surface hydrogen entry from an aqueous solution occurs for a much wider range of conditions than previously believed. Chloride ion and acidification indirectly promote hydrogen ion reduction and entry on the recessed surface through their direct effect on promoting the IR-induced mechanism of crevicing.

14. SUBJECT TERMS

KEY WORDS: modeling of hydrogen electro permeation, diffusion of hydrogen, hydrogen absorption, chloride ion and acidification effects, hydrogen evolution in recesses.

15. NUMBER OF PAGES

16. PRICE CODE

17. SECURITY CLASSIFICATION OF REPORT	18. SECURITY CLASSIFICATION OF THIS PAGE	19. SECURITY CLASSIFICATION OF ABSTRACT	20. LIMITATION OF ABSTRACT
UNCLASSIFIED	UNCLASSIFIED	UNCLASSIFIED	

CONTENTS

INTRODUCTION

This report is divided into three selections. Section 1 is a summary of progress and a list of project publications in the past year. Section 2 is a report (reprint) on how to obtain the important hydrogen absorption (entry) and desorption* (exiting) rate constants from steady state hydrogen permeation data. Section 3 consists of two reprints, one that relates to the role of acidification and the other to the role of chloride ions in shifting the electrode potential inside a recess in the direction favoring proton reduction and hydrogen entry, and which present a combination of in-situ techniques: direct viewing of the crevice wall (through a transparent media that forms the other wall of the crevice) and simultaneously using an adjustable potential measuring probe inside the crevice.

SECTION 1

PROGRESS SUMMARY

The problem of hydrogen-induced damage and failure of metallic systems starts with hydrogen entry. The hydrogen permeation technique has been successfully used for three decades for determining some of the important hydrogen/material parameters, e.g., the hydrogen diffusivity and hydrogen concentration inside the input surface, but most of the parameters related to hydrogen entry were not previously attainable from permeation data because of the incomplete nature of the quantitative treatment of hydrogen permeation available in the literature. Our work of the past few years on the project corrected this situation so now a more rigorous quantitative treatment of the permeation process is available (described in last year's Annual Report and various publications). As a result several additional parameters related to hydrogen entry became attainable from permeation data. These are the proton discharge rate constant, transfer coefficient and exchange current density, the hydrogen recombination rate constant, the hydrogen coverage, and the ratio of (but not the individual) hydrogen absorption and desorption rate constants. To obtain the individual absorption and desorption constants some further model development was required, and has recently been accomplished. This extension of the model

---

* The desorption or exiting rate constant is referred to as the adsorption rate constant in the reprint.

requires that the steady state permeation data are obtained as a function of membrane thickness. This extension of the model is described in Section 2.

The scanning tunneling microscope provides the opportunity for in-situ imaging of the surface over a wide range of scale including the atomic scale. Imaging adsorbates on surfaces is also possible. Initial STM studies on the project began with the easy-to-study silicon low index single crystal surfaces using the ultra high vacuum STM. Then, studies of hydrogen adsorption on these surfaces was started with the initial successful STM observations at the atomic level reported last year for the Si 111(7x7) surface (ONR Technical Report, February 1990). This initial success in imaging adsorbed hydrogen atoms is encouraging for the successful development of the STM technique, and alternatively the atomic force microscope (AFM) which we are now employing in our studies of adsorbed monolayers, for in-situ imaging of hydrogen adsorption on metals at the atomic level.

For most cases of nonuniform corrosion, the electrode potential varies over the surface, e.g., in the case of oxygen concentration cells, being more noble at cathodic sites of high oxidant availability and more negative at anodic sites. The shift of the electrode potential in the negative direction can be quite large and its magnitude is unknown in service applications since the anodic sites are in recesses (crevices, cracks, etc.). It follows that the tendency for the occurrence of the hydrogen evolution reaction, and thus for hydrogen entry into the metal structure, is greatest in the recesses.

Thus, it becomes important to know how and to what extent the various parameters e.g., acidification of the local cell environment, associated with recesses in particular during localized corrosion, affect the shift of the local electrode potential in the negative direction. This question does not appear to have been addressed in the literature but is not trivial as we now know from recent results on crevice corrosion of iron. During crevicing ever more negative electrode potentials to a limiting value exist along the crevice wall with increasing depth into the crevice, accompanied by the evolution of hydrogen gas (ONR Technical Reports, February 1988, January 1988 and October 1987, and reprints in Section 3 of this report). During the past year the roles of acidification, chloride ion, recess geometry, and other factors, on promoting the potential shift into the hydrogen evolution potential region within recesses have been under study. Both acidification and chloride ion have been found to increase the magnitude and

frequency of the potential shift within recesses in the negative direction. Thus, the tendency for hydrogen evolution and entry into the metal within recesses is increased by both of these parameters along with the tendency for localized corrosion. Results available to date are presented in Section 3.

PUBLICATIONS ON THE PROJECT

R. N. Iyer and H. W. Pickering, "Construction of Iso-Coverage Tafel Plots to Evaluate the True H. E. R. Transfer Coefficient", J. Electrochem. Soc., 137, 3512-3514 (1990).

K. Cho and H. W. Pickering, "Demonstration of Crevice Corrosion in Alkaline Solution Without Acidification", J. Electrochem. Soc., 137, 3313 (1990).

R. Iyer and H. W. Pickering, "Current Developments in Modeling and Characterizing Electrochemically Influenced Hydrogen Evolution and Entry in to Materials", pp. 195-209 in Hydrogen Effects on Material Behavior N. R. Moody and A. W. Thompson, ed., TMS, Warrendale, PA (1990).

R. N. Iyer and H. W. Pickering, "Mechanism and Kinetics of Electrochemical Hydrogen Entry and Degradation of Metallic Systems", Annual Review of Materials Science, Vol. 20, Annual Reviews, Inc., Palo Alto, Calif., (1990).

A. Valdes and H. W. Pickering, "IR Drops and the Local Electrode Potential During Crevicing of Iron", pp. 393-401 in Advances in Localized Corrosion, H. S. Isaacs, U. Bertocci, J. Kruger and S. Smialowska, eds., NACE-9, National Association of Corrosion Engineers, Houston, Texas (1990).

H. W. Pickering, "A Critical Review of IR Drops and Electrode Potentials Within Pits, Crevices and Cracks, ibid, pp. 77-84.

H. W. Pickering and T. Sakurai "Scanning Tunneling Microscopy and Its Applications in Corrosion Science", Sym. on Surface and Interface Characterization in Corrosion, NACE, Houston, Texas, Preprint No. 81, CORROSION 91.

SECTION 2

HYDROGEN PERMEATION MODELING

Construction of Iso-Coverage Tafel Plots to Evaluate the HER Transfer Coefficient

Rajan N. Iyer and Howard W. Pickering*

*Department of Materials Science and Engineering, The Pennsylvania State University,
University Park, Pennsylvania 16802*

This communication is a supplement to a recent paper (1) describing a new model of electrolytic hydrogen charging and permeation in metals. This model shows how the forward and backward rate constants of the hydrogen entry step, k_{abs} and k_{ads}, respectively, can be obtained from permeation data as a function of membrane thickness, and that the hydrogen evolution reaction (h.e.r.) transfer coefficient, α, should perhaps not be considered a constant for the entire range of hydrogen coverage, θ_H, on metallic surfaces. In the present paper we show that if, in addition, experiments are conducted for membranes of certain, rather than random, thicknesses, the α values at constant hydrogen coverage can also be obtained.

For even small variations of α with θ_H, iso-coverage α values are needed in the newly developed (I-P-Z) model (1, 2) in order to accurately determine the above-mentioned and other previously unobtainable parameters of the h.e.r. and hydrogen permeation processes. And it has been previously pointed out that the value of α is important in determining the polarizability of the electrolytic reduction of protons to form adsorbed hydrogen atoms on a metallic electrode surface (3, 4). Especially when the surface hydrogen coverage is significant ($\theta_H \gtrsim 0.1$), corresponding to significant percentages (>2% for iron) (1) of the charging current (i_c) permeating through the membrane, rather than evolving as hydrogen gas, it will not be possible to evaluate α from the conventional Tafel plot, log i_c vs. η, since these plots will not be straight lines. This perhaps suggests the influence of θ_H on α. Examples of non-straight Tafel plots are shown elsewhere (5-7). Since they occur for a wide range of hydrogen coverage, including very low θ_H, it now seems reasonable to consider, as we are doing in this note, that for some conditions α may vary significantly with θ_H. In the following analysis, a novel technique for analysis of hydrogen permeation data as a function of thickness is advanced to enable construction of Tafel plots as iso-coverage lines from which α (at constant θ_H) can be accurately evaluated.

The Butler-Volmer equation for hydrogen discharge when the backward reaction can be neglected ($\eta >> RT/F$) is (1, 3, 4)

$$i_c = i'_o (1 - \theta_H) e^{-a\alpha\eta} \qquad [1]$$

where i_c is the cathodic current density,

$i'_o = \dfrac{i_o}{(1 - \theta_e)}$,

i_o = exchange current density,

θ_e = equilibrium surface H coverage,

θ_H = (polarized) surface H coverage,

$a = \dfrac{F}{RT} = 38.94 \text{ V}^{-1}$,

α = h.e.r. transfer coefficient,

η = H overvoltage = polarization,

F = Faraday constant,

* Electrochemical Society Active Member.

R = gas constant, 8.314 J (g-mol K)$^{-1}$, and

T = temperature, K.

Equation [1] can be rewritten as

$$\theta_H = 1 - \frac{i_c e^{a\alpha\eta}}{i'_o} \qquad [2]$$

Equation [2] can be termed the polarized adsorption isotherm for a reaction sufficiently far from equilibrium so that the back-reaction can be neglected (1). Differentiating Eq. [2] with respect to η and simplifying

$$\frac{d\theta_H}{d\eta} = - \frac{i_c e^{a\alpha\eta}}{i'_o} \left(a\alpha + \frac{d \ln i_c}{d\eta} \right) \qquad [3]$$

Equation [3] shows that if the coverage, θ_H, can be fixed while polarizing the electrode, i.e., if θ_H = constant, then $d\theta_H/d\eta = 0$ and

$$\alpha(\theta_H \text{ constant}) = - \frac{1}{a} \frac{d \ln i_c}{d\eta} = - \frac{RT}{2.303F} \frac{d \log i_c}{d\eta} \qquad [4]$$

where α (θ_H constant) is the h.e.r. transfer coefficient obtained at a particular θ_H coverage. Equation [4] is the familiar Tafel equation, except that $d\theta_H/d\eta = 0$ has been applied as a condition to obtain an actual α value.

The normal tendency for θ_H to increase with increasing η (in the absence of permeation into the metal) can be controlled by decreasing the membrane thickness, L, thereby increasing the steady-state permeation flux, j_∞ (or equivalently the permeation current, i_∞), in hydrogen permeation experiments utilizing the Devanathan-Stackurski cell (8), i.e., the i_∞ value can be manipulated by varying L. This is possible because the steady-state hydrogen permeation through the bulk metal can be described as a simple rate-controlling diffusion process (8) and i_∞, θ_H, and L are related by (1)

$$\theta_H = \frac{L}{FD_l} \frac{i_\infty}{k''} \qquad [5]$$

where

D_l = the bulk hydrogen diffusivity in the metal, and

k'' = the thickness-dependent hydrogen absorption-adsorption constant = $k_{abs}/[k_{ads} + D_l/L]$.

Rearranging k'' gives

$$\frac{1}{k''} = \frac{1}{k'} + \frac{D_l}{k_{abs}} \cdot \frac{1}{L} \qquad [6]$$

where k' = the (thickness-independent) hydrogen absorption-adsorption constant under conditions of negligible permeation = k_{abs}/k_{ads}.

It is now apparent from Eq. [5] that we can achieve a constant θ_H (termed the iso-coverage) condition by setting $i_\infty L$

$(k'')^{-1}$ = constant. Then, using Eq. [5] and [6] one can prove that

$$i_{x,n} = i_{x,m}[1 + (L_m - L_n)(L_n + (D_1/k_{ads}))^{-1}] \qquad [7]$$

where $i_{x,n}$ and $i_{x,m}$ refer to i_x values for membranes n and m of thicknesses L_n and L_m. Equation [7] is applicable to any number of membranes, N, of different thickness where m = 1,2,3, ... ; n = 2,3,4, ... N; and n > m. Equation [7] describes the relationship between the iso-coverage i_x values for membranes n and m. However, we have to know the D_1/k_{ads} value or eliminate this unknown quantity from Eq. [7] with other known quantities, as done below.

If the h.e.r. occurs by a discharge-recombination process and if the (chemical) recombination process is not rate-limiting, it has been shown (1) that

$$i_x = Ki_r^{1/2} = K(i_c - i_x)^{1/2} \qquad [8]$$

where K is a function of L. Since i_r is constant (for constant θ_H) and independent of L, it follows from Eq. [7] and [8] that

$$i_{x,n} = (K_n/K_m) i_{x,m} \qquad [9]$$

where K_n and K_m refer to the K values for membrane thicknesses of L_n and L_m, respectively. It may be noted that K is a constant for each of the membranes. From Eq. [8] and [9], one obtains after simplification

$$i_{c,n} = i_{c,m} + ((K_n/K_m) - 1) i_{x,m} \qquad [10]$$

Equation [10] can thus be used recursively to find iso-coverage $i_{c,n}$ (and hence η_n) values from polarization and permeation measurements on membranes with varying thickness. Since K is inversely proportional to L, it is clear that $K_n/K_m \neq 1$. This means that different iso-coverage i_c (and hence η) values, can be obtained from Eq. [10] by using membranes of different thickness. But it is necessary to vary the thickness by one to two orders of magnitude depending on the magnitude of i_x. Since i_x will best be obtained for a number of i_c values, i_c should always be low enough to avoid introducing nonsaturable traps, and should be applied in a sequence of decreasing magnitudes in order to have a stable trap density and to minimize film effects. The presence of a film will also have to be determined as described elsewhere (9, 10) in order to know if hydrogen is adsorbing on a film or on the metal surface.

If the assumptions in Eq. [8] (1) are not met, for example if the h.e.r. occurs by a more complex process such as discharge followed by simultaneous chemical and electrochemical desorption, or if the recombination process is rate-limiting, then Eq. [8] will be modified. An example of a modified relationship between i_x and i_r occurs for the case of H_2S poisoning the h.e.r. and enhancing hydrogen entry into iron in acidic solutions (7, 9) for which the relationship is ln $(\sqrt{i_r}/i_x) = (a fb/k'') i_x + $ ln $\{b(Fk_3)^{0.5}/k''\}$. Since this relationship contains the unknowns a and k'', it cannot be used to find D_1/k_{ads}. Instead, an alternative procedure has to be used as follows.

From Eq. [5] and [6], one can obtain

$$\theta_H = \frac{i_x}{FD_1}\left[\frac{L}{k'} + \frac{D_1}{k_{abs}}\right]$$

i.e.

$$FD_1 \cdot k' \cdot \theta_H \cdot \frac{1}{i_x} = L + \frac{D_1}{k_{ads}}$$

since

$$\frac{k'}{k_{abs}} = \frac{1}{k_{ads}}$$

or

$$g \cdot \frac{1}{i_x} = L + \frac{D_1}{k_{ads}} \qquad [11]$$

where

$$g = FD_1 k' \theta_H \qquad [11a]$$

At equilibrium of the h.e.r., i_x is small but finite, corresponding to the equilibrium hydrogen coverage, θ_e, *i.e.*, at $\eta = 0$, $i_x = i_x^o$; $\theta_H = \theta_e$; $g = g^o$. Then, Eq. [11] becomes

$$L = \frac{g^o}{i_x^o} - \frac{D_1}{k_{ads}} \qquad [11b]$$

Whereas θ_e is considered to be independent of L, i_x^o depends on L. By plotting L *vs.* $1/i_x^o$ (where i_x^o is obtained by extrapolating the i_x *vs.* η plot to $\eta = 0$), we can evaluate $g^o =$ the slope, and $-D_1/k_{ads} =$ intercept. This value of $-D_1/k_{ads}$ can be used in Eq. [7] to calculate iso-coverage i_x values recursively for various membranes.

It is to be noted that data need to be obtained on membranes whose thicknesses span one or two orders of magnitude. Depending on the hydrogen diffusivity, membranes with thicknesses ranging from about 50 μm to 5 mm can be used. Still, it may be that the intercept of L *vs.* $1/i_x^o$ is undeterminable by extrapolation. In these cases (with $\theta_e > 0$), one may instead use the slope, g^o. It can be easily shown using Eq. [11] for iso-coverage of two membranes, m and n, that

$$\frac{1}{i_{x,n}} = \frac{1}{i_{x,m}} + \frac{(L_n - L_m)}{g_m} \qquad [11c]$$

where $g_m = g_n$ (Eq. [11a]) since $\theta_{H,m} = \theta_{H,n}$ (iso-coverage). Again, using Eq. [11] and [11b] for membrane m, one can show that

$$\frac{g_m}{i_{x,m}} = \frac{g^o}{i_{x,m}^o} \qquad [11d]$$

From Eq. [11c] and [11d]

$$i_{x,n} = \frac{i_{x,m}}{\left[1 + \left\{(L_n - L_m)\left(\frac{i_{x,m}^o}{g^o}\right)\right\}\right]} \qquad [12]$$

Once iso-coverage i_x values are obtained on different membranes (by recursively using Eq. [10] or alternatively using Eq. [7] or [12] in conjunction with L *vs.* $1/i_x^o$ and Eq. [11b], corresponding iso-coverage η (*i.e.* η_n) and i_c (*i.e.* $i_{c,n}$) values are easily obtained. Thus $d\theta_{H,n}/d\eta_n = 0$ ($\theta_{H,n}$ representing iso-coverage) and Eq. [4] will hold as

$$\alpha(\theta_H \text{ constant}) = \frac{-RT}{2.303F}\frac{\Delta \log i_{c,n}}{\Delta \eta_n} = \frac{RT}{2.303F}\frac{\Delta \log i_{c,n}}{\Delta(-\eta)} \qquad [13]$$

The iso-coverage Tafel plots (log $i_{c,n}$ *vs.* η_n) will yield the α values for the different hydrogen coverages, θ_H. The advantage of using α (θ_H constant) is in reducing the scatter in log i_c *vs.* η and $i_c e^{a\alpha \eta}$ *vs.* i_x plots for the I-P-Z model (1), and thus yielding more accurate values of the various rate constants, surface coverages, etc. In reactions where significant coverages as well as both chemical recombination and electrochemical recombination rates for the h.e.r. are prevalent, such as in poisoned electrolytes (7, 9), it may become mandatory to use the iso-coverage Tafel plots, derived here, to determine α.

In conclusion, iso-coverage Tafel plots should be used to determine the most accurate α values, especially if coverages are significant. The data base needed for this construction is simply the measured cathodic overvoltage (η), cathodic current density (i_c), and steady-state permeation current (i_x) for membranes with one to two orders ($\sim$50 μm to 5 mm) of variation in thickness.

Acknowledgments

REFERENCES

1. R. N. Iyer, H. W. Pickering, and M. Zamanzadeh, *This Journal*, **136**, 2463 (1989).
2. R. N. Iyer, H. W. Pickering, and M. Zamanzadeh, *Scr. Metall.*, **22**, 911 (1988).
3. E. Gileadi, K. Kirowa-Eisner, and J. Penciner, "Interfacial Electrochemistry," pp. 54, 109-111, Addison-Wesley, Reading, MA (1975).
4. J. O'M. Bockris and A. K. N. Reddy, "Modern Electrochemistry," Vol. 2, pp. 918, 1007, Plenum Press, New York (1970).
5. C. Kato, H. J. Grabke, B. Egert, and G. Panzner, *Corros. Sci.*, **24**, 591 (1984).
6. E. G. Dafft, K. Bohnenkamp, and H. J. Engell, *ibid.*, **19**, 591 (1979).
7. R. N. Iyer, I. Takeuchi, M. Zamanzadeh, and H. W. Pickering, *Corrosion*, **46**, 460 (1990).
8. M. A. Devanathan and L. Stackurski, *This Journal*, **111**, 619 (1964).
9. R. N. Iyer and H. W. Pickering, *Annu. Rev. Mater. Sci.*, Vol. 20, p. 299, Annual Reviews Inc., Palo Alto, CA (1990).
10. R. N. Iyer and H. W. Pickering, In preparation.

SECTION 3

RECESSED SURFACES

- ROLE OF ACIDIFICATION
- ROLE OF CHLORIDE IONS

Demonstration of Crevice Corrosion in Alkaline Solution Without Acidification

K. Cho* and H. W. Pickering**

Department of Materials Science and Engineering, The Pennsylvania State University, University Park, Pennsylvania 16802

Brown, et. al. (1) showed that significant changes in pH occurred inside cracks. Then Pickering and co-workers (2-4) showed the same for electrode potential, E, inside pits and, even more clearly, inside crevices. Although generally under recognized, the importance of E in stabilizing local cells has gained in stature over the years so that today E is considered as important as pH. The roles of pH and E in stabilizing localized corrosion are shown in Fig. 1. Acidification within the crevice causes the passivation potential, E_{pp}, to move to the right, thereby extending the active region of the crevice electrolyte towards the outer surface potential, $E(x=o)$. Alternatively, $E(x)$ is a function of distance x into the crevice, shifting in the less oxidizing direction or to the left in Fig. 1. Hence, at some distance into the crevice, $E(x)$ is in the active region. In the limit, either the shift in pH or in E can solely stabilize the local cell process, whereas in general both E and pH participate in the stabilization. A criterion for the occurrence of stable local cell action is that $IR \geq IR^*$ (Fig. 1) since $E(x) = E(x=o) - IR$, where IR^* is determined by E_{pp} which is strongly pH dependent and by $E(x=o)$, and IR is determined by the factors associated with charge transport in electrolytes (3,4).

Following the recognition that large $E(x)$ gradients contribute to the stability and mechanism of local cell processes (2), Valdes (3,4) measured large $E(x)$ gradients within crevices in iron in acid solution (pH 2.8) for which there is no tendency for hydrolysis and in buffered acid solution (pH 4.6) for which the hydrolysis tendency is suppressed by the buffer. In these experiments for which the solution was already acid and acidification per se was not a factor, he found that active crevicing only occurred when the $IR>IR^*$ condition was met. Furthermore, in the absence of an active loop in the polarization curve as is generally true for iron in alkaline solution, active crevicing did not occur unless strong acidification occurred. In this case, acidification is needed to form an active loop thereby making it possible to meet the $IR \geq IR^*$ condition. Conversely, if an active loop exists in an alkaline solution, crevicing should occur even without acidification. The iron/ammoniacal solution is perhaps unique in this regard in that an active loop exists at pH 9 to 10 (Fig. 1). Also,

the strongly iron complexing ammoniacal species and its strong buffering action both preclude hydrolysis, so that no significant acidification can be expected.

EXPERIMENTAL

Pure iron (Ferrovac E) and $1M\ NH_4OH$ -$1M$ NH_4NO_3 solution were used and the experimental set-up and sample arrangement are shown in Fig. 2. The crevice consisted of one metallic side, four inert (plexiglass) walls and one opening to the bulk solution. The crevice width was larger in the upper section with dimensions 0.05 cm x 0.5 cm x 0.5cm and the lower narrower section, 0.001 cm x 0.5 cm x 0.5 cm. In preliminary experiments it was found that crevicing only occurred in the narrower section where the condition IR $\geq IR^*$ was met. Lacquer was used to eliminate crevices between the iron and Teflon holder. Observations of the events inside the crevice and photographing them was possible with a stereomicroscope. Luggin-capillaries were used to monitor $E(x=o)$ in the passive region on the outer surface and $E(x)$ inside the crevice. Reproducible results have been obtained using a Luggin measuring probe with a diameter 0.005 cm, to measure local potentials in crevices of the same dimensions (3,6). A silver oxide electrode was developed into a microprobe for monitoring the pH inside the crevice. It was confirmed using buffer solutions of different pH that its equilibrium potential was a linear function of pH. Thus, both $E(x)$ and pH could be measured as a function of the depth x within the upper segment of the crevice but not in the lower segment because of its narrow opening. The pH was also measured by extracting solution with a syringe and along the crevice wall by applying pH papers.

RESULTS

With the outer top surface of the iron sample anodically polarized in the passive region at +200 mV, SCE, as illustrated in Fig. 1, the dissolution processes observed on the iron crevice wall are shown in Fig. 3. The horizontal line halfway down (x=0.5 cm) the crevice wall is the boundary between the two segments of the crevice and the vertical white line down the middle is the fine Luggin-capillary used to measure the electrode potential at the halfway mark, $E(x=0.5\ cm)$. The outer(top) surface of the iron sample is in the passive region, as is the crevice wall down to the (lower)

horizontal line (x≅0.7 cm) indicated by the arrow in the 16 hour photograph of Fig. 3. Below the arrow (brighter region) iron is dissolving or crevicing. In this region a dark-green corrosion product and an increasingly aggressive dissolution were observed. The latter was also indicated by an increasing current flowing out of the crevice with time, as shown in Fig. 4. The time dependent electrode potential, E(x=0.5 cm), at the opening of the narrower crevice is also shown in Fig. 4. At 18 hr, E(x=0.5 cm) is almost 600 mV less oxidizing than E(x=o) at the outer passivated surface, and it can be easily inferred that at a greater depth into the (narrower) crevice (specifically below the arrow in Fig. 3), E(≥0.7 cm) < E_{pp}, so that active iron dissolution or crevicing occurs. In this experiment a 1:1 correspondence between active crevicing and a sharp E(x) gradient, so that IR > IR*, was always observed. The measured pH of the crevice solution was always the same within the experimental error (approx. ± 0.5 pH unit) as the bulk (pH = 9.7) solution.

REFERENCES

1. B.F. Brown, C.T. Fujii and E.P. Dahlberg, *This Journal*, 116, 218 (1969).
2. H. W. Pickering and R. P. Frankenthal, *This Journal*, 119, 1297, 1304 (1972).
3. A. Valdes and H. W. Pickering, in Advances in Localized Corrosion (ed. H. Isaacs, et. al.) NACE, Houston, in press; H. W. Pickering, ibid.
4. H. W. Pickering, Corrosion Sci., 29, 325 (1989)
5. J. W. Lee, K. Osseo-Asare and H. W. Pickering, *This Journal*, 132, 550 (1985).
6. B. G. Ateya and H. W. Pickering, *This Journal*, 122, 1018 (1975).

Fig. 2. Experimental set-up.

6 hr   **16 hr**

Fig. 3. Photographs of iron crevice wall. E(x=o) = +200 mV, SCE (top surface).
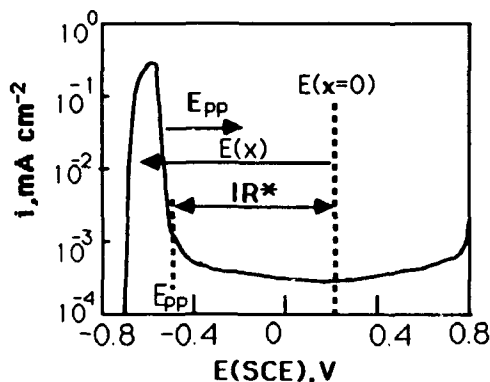
Fig. 1. Anodic polarization curve of iron in deaerated ammoniacal solution, pH 9.7, 0.1 mV s^{-1} (5).

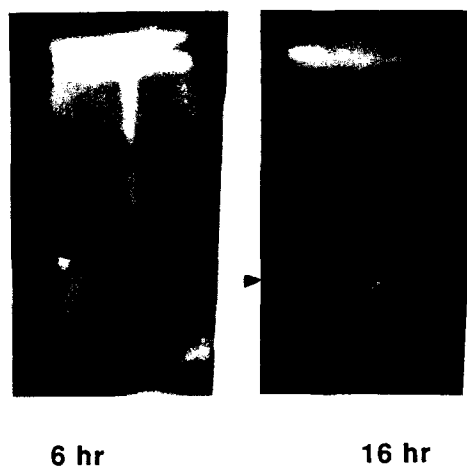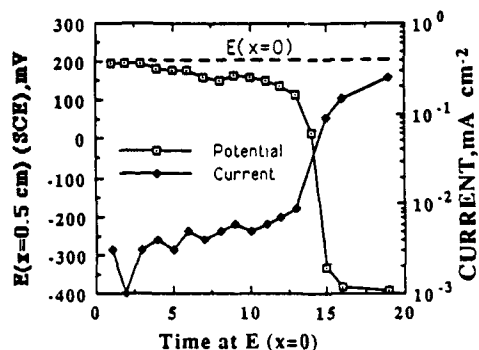Fig. 4. E(x=0.5 cm) and current flowing out of crevice as a function of time.

The Role of Chloride Ions in the IR > IR* Criterion for Crevice Corrosion in Iron

K. Cho* and H. W. Pickering**

Department of Materials Science and Engineering, The Pennsylvania State University, University Park, Pennsylvania 16802

ABSTRACT

Although chloride ions have long been known to promote crevice corrosion in metals, little detailed understanding is available In this paper, measurements of the potential, pH. and current inside the crevice, and simultaneous viewing of the crevice wall through a transparent portion of the crevice, have provided new results, and understanding of the role of chloride in promoting crevice corrosion. The results also are a proof of the potential shift theory of crevice corrosion.

Acidification (of neutral or alkaline solutions) and a buildup of the so-called aggresive ions, e.g., Cl ions, occur inside crevices of iron, and both promote the crevicing process (1-3). Recently, it has been shown that i.) relatively large IR drops, sufficient to shift the electrode potential within the crevice into the active region, are necessary for crevicing to occur in iron (4-7); and ii.) acidification promotes crevicing by enlarging the active loop (the active/passive potential shifts to more noble values), and is sometimes necessary to create an active loop, but is not in the case of acid and some alkaline solutions for which an active loop is already present (4-7). An example system in which crevicing occurs in the absence of acidification is iron in the alkaline ammoniacal solution. for which an active loop exists in the alkaline region because of the stable iron

amine complex ion. It was found that crevicing occurs in this system when the electrode potential at the crevicing site shifts into the active region, and that the pH holds constant in the crevice at the pH 9.8 bulk value (6). In these experiments on the IR drop criterion for crevicing and on the role of acidification (4-7), there were no chlorides present in the solutions, so it is clear that chloride anions are not necessary for crevicing to occur in iron over the acid-to-alkaline pH range. Nevertheless, it is known that Cl ion promotes the crevicing process. The purpose of the present paper is to investigate the role of chloride in the crevicing process using the same experimental procedure that has led to the above-mentioned identification of the IR drop mechanism of crevicing and improved understanding of the role of acidification in the crevicing process.

Thus. crevice corrosion has been found to occur when $\Delta\phi$ $\Delta\phi^*$. where $\Delta\phi$ is the voltage drop in the electrolyte between
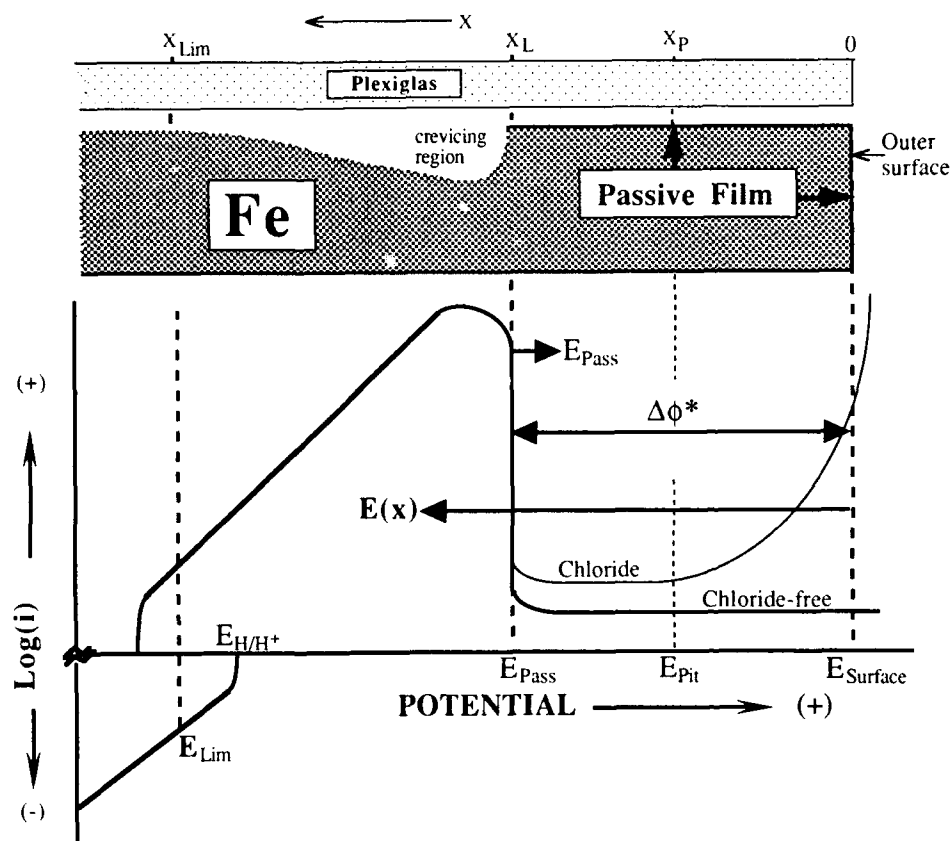
Fig. 1. Schematic of the potential shift mechanism of crevice corrosion.

the cathodic site at the outer surface (where oxygen is plentiful) and the crevicing site, and $\Delta\phi^*$ is defined in Fig. 1 as the difference between the cathodic site electrode potential, $E_{Surface}$, and the active/passive potential of the crevice electrolyte, E_{Pass}. The measurable voltage drop, $\Delta\phi$, is the product of the metal dissolution current flowing out of the crevice (in the $-x$ direction) and the resistance of the electrolyte path to current flow, i.e., $\Delta\phi = -IR$, and $IR > IR^*$ is equivalent to $\Delta\phi > \Delta\phi^*$. In practice, the deconvolution of the IR product is not trivial, since both the current flowing out of the crevice and the resistivity of the current path vary with distance x into the crevice. The latter is especially evasive because H_2 gas bubbles regularly form deep inside the crevice where $E_{(x)}$ is in the hydrogen evolution potential range, as indicated in Fig. 1. In some regions of the crevice, wall, $x_L < x < x_{Lim}$, in Fig. 1, the condition $\Delta\phi > \Delta\phi^*$ is met, meaning that $E(x)$ is in the active region, $E_{Pass} > E > E_{Lim}$. Here $E(x)$ is related to $\Delta\phi$ by the equation, $E(x) = E_{Surface} - \Delta\phi$. Acidification shifts E_{Pass} to significantly more noble potentials inside the crevice for most neutral and alkaline bulk solutions. As a result, $\Delta\phi^*$ is decreased and $\Delta\phi$ may be increased because larger metal dissolution rates can then occur in the active region. Thus, the condition $\Delta\phi > \Delta\phi^*$ is met more easily within the crevice as acidification occurs. In this paper we address the question: does Cl ion similarly decrease $\Delta\phi^*$ by shifting E_{Pass} in the noble direction, or does it increase $\Delta\phi$ (without an accompanying $\Delta\phi^*$ shift), and if so how?

Experimental

An iron/Plexiglas crevice (Fig. 2) described elsewhere (4, 5) was anodically polarized on the outer surface at +600 mV vs. saturated calomel electrode (SCE) (passive region) in a buffered (pH 4.6) solution containing chloride. This system is known to contain an active loop and to hold a constant pH (4.6 ± 0.5) inside the crevice during the crevicing process (4, 5). The crevice opening was 0.5 mm × 5 mm and the depth was 10 mm. Lacquer was used to eliminate crevices between the iron walls and the Teflon holder. The lacquer edges, themselves, underwent some inconsequential crevicing, and preferential pitting when the solution contained chloride anions. In situ observation of the crevicing action on the iron wall was accomplished through the transparent Plexiglas using a photographic camera with attached macro-lenses. A three-directional micrometer stage enabled precise positioning of the Luggin measuring probe at the opening of the crevice and

elsewhere inside the crevice, in order to monitor the local electrode potential inside the crevice as a function of position and time. The pH was measured by extracting solution with a syringe connected to a fine glass capillary and by applying pH papers along the crevice wall after disassembling. All of these procedures have been tested and described (4-8).

Results

During crevicing, the visual changes on the iron crevice wall were the same as reported previously (4-7), except pitting occurred on the outer surface and part way into the crevice to a certain distance along a horizontal front at x_p, as shown in Fig. 3. Figure 3b and other magnified photographs of the crevice wall were taken continually during the experiment. The simultaneously measured $E(x)$ value at the pitted/unpitted interface, x_p in Fig. 3, corresponds to E_{pit} (Fig. 1). The presence of the pitting front on the crevice wall (Fig. 3b) is another independent confirmation of the large potential distribution along the crevice wall during crevicing and its correspondence to the anodic polarization curve of the dissolving metal with its active and passive regions (4-7). The measured limiting poten-
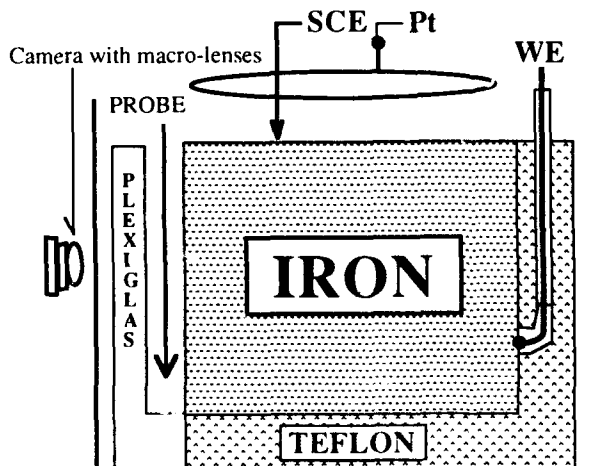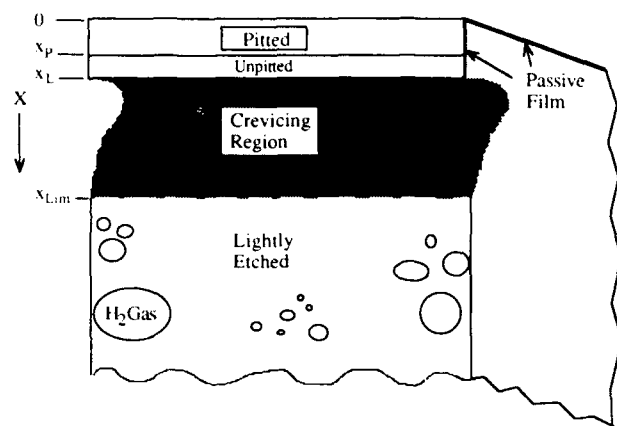

Fig. 2. Experimental set-up.

Fig. 3. Schematic (left) and photograph (right) of the iron crevice wall taken through the Plexiglas during anodic polarization of the outer surface at +600 mV vs. SCE in 0.5M CH$_3$COOH + 0.6M NaC$_2$H$_3$O$_2$ + 0.03M NaCl.

tial (E_{Lim}) (5) in the crevice was approximately 550 mV vs. SCE (Fig. 4), being about 35 mV more negative than the equilibrium potential for hydrogen evolution, consistent with the observed continuous formation of H$_2$ gas bubbles in the deeper regions of the crevice, as reported before (4-8). The potential gradient in the crevice, $\Delta\phi$, is thus as large as 1150 mV. H$_2$ gas bubbles were also observed coming continually out of the pits and adhering on the surface, confirming this sighting in a prior investigation (8) in which the gas was identified as hydrogen, a strong proof in itself that large potential shifts also exist within pits in iron.

Crevicing more readily occurred in the presence of Cl ions, as shown by the smaller x_L value: $x_L = 1.3$ and 0.7 mm for the chloride-free and chloride-containing solutions, respectively. Figure 4 shows the increase in current in the presence of chloride. Chloride anions were found to have a small effect on the potential of the active/passive transition: E_{Pass} shifted 30 to 40 mV in the noble direction when the electrolyte contained 0.01M chloride. This resulted in a modest decrease in $\Delta\phi^*$ and an increase in the size of the active loop. The latter, however,

can amount to a rather significant increase in the current flowing out of the crevice, since the peak active current increased a few mA cm^2 and, hence, so also would the metal dissolution rate at the crevice site ($x_L \cdot x \cdot x_{Lim}$). Other contributions to a larger current flowing out of the crevice are the observed pitting on the crevice wall at $x \cdot x_p$ (Fig. 3) and a higher passive current (schematically shown in the polarization curve in Fig. 1) located at $x \approx x_L$ on the crevice wall. The higher current causes a larger $\Delta\phi$ per unit length into the crevice, thereby yielding the $\Delta\phi \cdot \Delta\phi^*$ condition at a smaller x_L value. Thus, the shift in x_L to a smaller value is mainly due to a larger $\Delta\phi$, with a smaller contribution coming from the decrease in $\Delta\phi^*$. The measured constant pH values in the crevice showed that the buffering action was effective in the crevice and that the pH was not a variable in the above experiments. In brief, chloride anions promote the crevicing process by increasing the current flowing out of the crevice and, hence, increasing $\Delta\phi$, and to a lesser extent by decreasing $\Delta\phi^*$. Thus, based on the $\Delta\phi \cdot \Delta\phi^*$ criterion, one can predict that crevice corrosion will occur in shallower crevices or in crevices with a larger gap between the crevice walls when chloride anions are added to the solution.
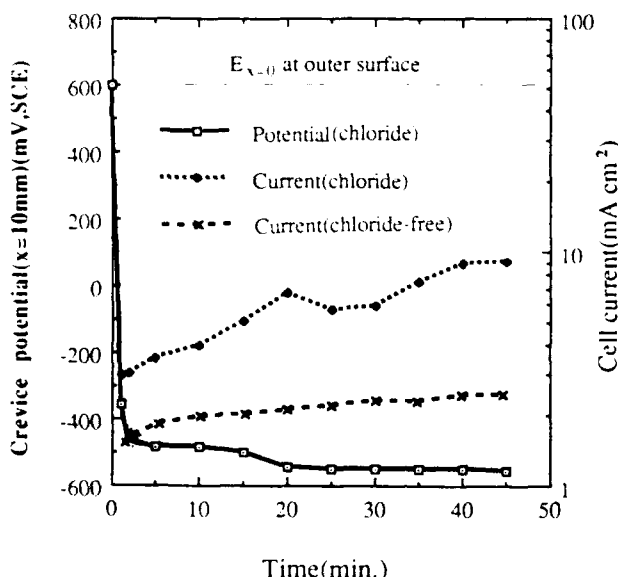
Acknowledgments

Fig. 4. Current flowing out of the crevice (includes outer surface contribution) and electrode potential at the bottom of the crevice, $E_{(x=10mm)}$, as a function of time for $E_{(x=0)}$ +600 mV vs. SCE.

REFERENCES

1. A. Pourbaix, *Corrosion*, **27**, 449 (1971).
2. G. Sandoz, C. T. Fujii, and B. F. Brown, *Corros. Sci.*, **10**, 829 (1970).
3. M. G. Fontana, "Corrosion Engineering," 3rd Ed., pp. 53-55, McGraw-Hill (1986).
4. A. Valdes and H. W. Pickering, in "Advances in Localized Corrosion," H. S. Isaacs, U. Bertocci, J. Kruger, and S. Smialowska, Editors, pp. 393-401, NACE, Houston (1990); H. W. Pickering, *ibid.*, pp. 77-84.
5. H. W. Pickering, *Corros. Sci.*, **29**, 325 (1989); Pickering, *Corrosion*, **42**, 125 (1986).
6. K. Cho and H. W. Pickering, *This Journal*, **137**, 3313 (1990).
7. H. S. Kim, Y. T. Kho, H. W. Pickering, and K. Osseo-Asare, *ibid.*, **138**, 1599 (1991).
8. H. W. Pickering and R. P. Frankenthal, *ibid.*, **119**, 1297 (1972).

Technical Reports and Publications   Feb 1990

Organization	Copies	Organization	Copies
Defense Documentation Center Cameron Station Alexandria, VA 22314	12	Naval Air Propulsion Center Trenton, NJ 08628 ATTN: Library	1
Office of Naval Research Dept. of the Navy 800 N. Quincy Street Arlington, VA 22217 ATTN: Code 1131	3	Naval Civil Engineering Laboratory Port Hueneme, CA 94043 ATTN: Materials Div.	1
Naval Research Laboratory Washington, DC 20375 ATTN: Codes 6000 6300 2627	1 1 1	Naval Electronics Laboratory San Diego, CA 92152 ATTN. Electronic Materials Sciences Division	1
Naval Air Development Center Code 606 Warminster, PA 18974 ATTN: Dr. J. DeLuccia	1	Commander David Taylor Research Center Bethesda, MD 20084	1
Commanding Officer Naval Surface Warfare Center Silver Spring, MD 20903-5000 ATTN: Library Code R33	1 1	Naval Underwater System Ctr. Newport, RI 02840 ATTN: Library	1
Naval Ocean Systems Center San Diego, CA 92152-5000 ATTN: Library	1	Naval Weapons Center China Lake, CA 93555 ATTN: Library	1
Naval Postgraduate School Monterey, CA 93940 ATTN: Mechanical Engineering Department	1	NASA Lewis Research Center 21000 Brookpark Road Cleveland, OH 44135 ATTN: Library	1
Naval Air Systems Command Washington, DC 20360 ATTN: Code 310A Code 5304B Code 931A	1 1 1	National Institute of Standards and Technology Gaithersburg, MD 20899 ATTN: Metallurgy Division Ceramics Division Fracture & Deformation Division	1 1 1

Office of Naval Research
Resident Representative
Ohio State University Research Center
1960 Kenny Rd
Columbus, OH 43210-1063

Naval Facilities Engineering Command Alexandria, VA 22331 ATTN: Code 03	1	Defense Metals & Ceramics Information Center Battelle Memorial Inst. 505 King Avenue Columbus, OH 43201

Naval Facilities Engineering
 Command
Alexandria, VA 22331
ATTN: Code 03   1

Commancant of the Marine Corps   1
Scientific Advisor
Washington, DC 20380
ATTN: Code AX   1

Army Research Office
P.O. Box 12211
Research Triangle Park, NC 27709
ATTN: Metallurgy & Ceramics
          Program   1

Army Materials Technology Laboratory
Watertown, MA 02172-0001
ATTN: Research Program Office   1

Air Force Office of Scientific
 Research
Building 410
Bolling Air Force Base
Washington, DC 20332
ATTN: Electronics & Materials
          Science Directorate   1

NASA Headquarters
Washington, DC 20546
ATTN: Code RM   1

Defense Metals & Ceramics
 Information Center
Battelle Memorial Inst.
505 King Avenue
Columbus, OH 43201   1

Oak Ridge National Laboratory
Metals and Ceramics Div.
P.O. Box X
Oak Ridge, TN 37380   1
Oak Ridge, TN 37380   1

Los Alamos Scientific Lab.
P.O. Box 1663
Los Alamos, NM 87544
ATTN: Report Librarian   1

Argonne National Laboratory
Metallurgy Division
 P.O. Box 229
Lemont, IL 60439   1

Brookhaven National Laboratory
Technical Information Division
Upton, Long Island
New York 11973
ATTN: Research Library   1

Lawrence Berkeley Lab.
1 Cyclotron Rd
Berkeley, CA 94720
ATTN: Library   1

David Taylor Research Ctr
Annapolis, MD 21402-5067
ATTN: Code 281   1
          Code 2813   1
          Code 0115   1

Supplemental Distribution List   Feb 1990

Profs. G.H. Meier and F.S.Pettit
Dept. of Metallurgical and
Materials Eng.
University of Pittsburgh
Pittsburgh, PA 15261

Dr. G. D. Davis
Martin Marietta Laboratories
1450 South Rolling Rd.
Baltimore, MD 21227-3898

Prof. H.K. Birnbaum
Dept. of Metallurgy & Mining Eng.
University of Illinois
Urbana, Ill 61801

⁵ Prof. P.J. Moran
Dept. of Materials Science & Eng.
The Johns Hopkins University
Baltimore, MD 21218

Prof. H.W. Pickering
Dept. of Materials Science and Eng.
The Pennsylvania State University
University Park, PA 16802

ᴰ Prof. J. Kruger
Dept. of Materials Science & Eng.
The Johns Hopkins University
Baltimore, MD 21218

Prof. D.J. Duquette
Dept. of Metallurgical Eng.
Rensselaer Polytechnic Inst.
Troy, NY 12181

Dr. B.G. Pound
SRI International
333 Ravenswood Ave.
Menlo Park, CA 94025

Prof. D. Tomanek
Michigan State University
Dept. of Physics and Astronomy
East Lansing, MI 48824-1116

Prof. C.R. Clayton
Department of Materials Science
& Engineering
State University of New York
Stony Brook
Long Island, NY 11794

Dr. M. W. Kendig
Rockwell International Science Center
1049 Camino Dos Rios
P.O. Box 1085
Thousand Oaks, CA 91360

Dr. J. W. Oldfield
Cortest Laboratories Ltd
23 Shepherd Street
Sheffield, S3 7BA, England

Prof. R. A. Rapp
Dept. of Metallurgical Eng.
The Ohio State University
116 West 19th Avenue
Columbus, OH 43210-1179

Prof. Boris D. Cahan
Dept. of Chemistry
Case Western Reserve Univ.
Cleveland, Ohio 44106

Dr. R. W. Drisko
Code L-52
Naval Civil Engineering Laboratory
Port Hueneme, CA 93043-5003

Prof. G. Simkovich
Dept. of Materials Science & Eng.
The Pennsylvania State University
University Park, PA 16802

Dr. R.D. Granata
Zettlemoyer Center for Surface Studies
Sinclair Laboratory, Bld. No. 7
Lehigh University
Bethlehem, PA 18015

Prof. M.E. Orazem
Dept. of Chemical Engineering
University of Florida
Gainesville, FL 32611

Dr. P. S. Pao
Code 6303
Naval Research Laboratory
Washington, D.C. 20375

Dr. M. S. Bornstein
United Technologies Research Center
East Hartford, CT 06108

Prof. R. M. Latanision
Massachusetts Institute of Technology
Room 8-202
Cambridge, MA 02139

Dr. R. E. Ricker
National Institute of Standards and
 Technology
Metallurgy Division
Bldg. 223, Room B-266
Gaithersburg, MD 20899

Dr. F. B. Mansfeld
Dept. of Materials Science
University of Southern California
University Park
Los Angeles, CA 90089

Dr. W. R. Bitler
Dept. of Materials Sci. and Eng.
115 Steidle Building
The Pennsylvania State University
University Park, PA 16802

Dr. S. Smialowska
Dept. of Metallurgical Engineering
The Ohio State University
116 West 19th Avenue
Columbus, OH 43210-1179

Dr. R. V. Sara
Union Carbide Corporation
UCAR Carbon Company Inc.
Parma Technical Center
12900 Snow Road
Parma, Ohio 44130

Prof. G.R. St. Pierre
Dept. of Metallurgical Eng.
The Ohio State University
116 West 19th Avenue
Columbus, Oh 43210-1179

Dr. E. McCafferty
Code 6322
Naval Research Laboratory
Washington, D. C. 20375

Prof. J. O'M. Bockris
Dept. of Chemistry
Texas A & M University
College Station, TX 77843

Dr. V. S. Agarwala
Code 6062
Naval Air Development Center
Warminster, PA 18974-5000

Prof. Harovel G. Wheat
Dept. of Mechanical Engineering
The University of Texas
ETC 11 5.160
Austin, TX 78712-1063

Prof. S. C. Dexter
College of Marine Studies
University of Delaware
700 Pilottown Rd.
Lewes, DE 19958